Tenascin-C restricts reactive astrogliosis in the ischemic brain

Egor Dzyubenko [a,#], Daniel Manrique-Castano [a,b,#], Matthias Pillath-Eilers [a], Paraskevi Vasileiadou [a], Jacqueline Reinhard [b], Andreas Faissner [b] and Dirk M Hermann [a]

***a* - Department of Neurology and Center for Translational Neuro- and Behavioral Sciences (C-TNBS),** *University Hospital Essen, Hufelandstraße 55, Essen D-45122, Germany*
***b* - Department of Cell Morphology and Molecular Neurobiology,** *Faculty of Biology and Biotechnology, Ruhr University Bochum, Universitätsstraße 150, Bochum D-44801, Germany*

Corresponding author. ***dirk.hermann@uk-essen.de.***
https://*doi.org/10.1016/j.matbio.2022.04.003*

Abstract

Cellular responses in glia play a key role in regulating brain remodeling post-stroke. However, excessive glial reactivity impedes post-ischemic neuroplasticity and hampers neurological recovery. While damage-associated molecular patterns and activated microglia were shown to induce astrogliosis, the molecules that restrain astrogliosis are largely unknown. We explored the role of tenascin-C (TnC), an extracellular matrix component involved in wound healing and remodeling of injured tissues, in mice exposed to ischemic stroke induced by transient intraluminal middle cerebral artery occlusion. In the healthy adult brain, TnC expression is restricted to neurogenic stem cell niches. We previously reported that TnC is upregulated in ischemic brain lesions. We herein show that the de novo expression of TnC post-stroke is closely associated with reactive astrocytes, and that astrocyte reactivity at 14 days post-ischemia is increased in TnC-deficient mice ($TnC^{-/-}$). By analyzing the three-dimensional morphology of astrocytes in previously ischemic brain tissue, we revealed that $TnC^{-/-}$ reduces astrocytic territorial volume, branching point number, and branch length, which are presumably hallmarks of the homeostatic regulatory astrocyte state, in the post-acute stroke phase after 42 days. Interestingly, $TnC^{-/-}$ moderately increased aggrecan, a neuroplasticity-inhibiting proteoglycan, in the ischemic brain tissue at 42 days post-ischemia. *In vitro* in astrocyte-microglia cocultures, we showed that $TnC^{-/-}$ reduces the microglial migration speed on astrocytes and elevates intercellular adhesion molecule 1 (ICAM1) expression. Post-stroke, $TnC^{-/-}$ did not alter the ischemic lesion size or neurological recovery, however microglia-associated ICAM1 was upregulated in $TnC^{-/-}$ mice during the first week post stroke. Our data suggest that TnC plays a central role in restraining post-ischemic astrogliosis and regulating astrocyte-microglial interactions.

Introduction

Glial responses fundamentally control successful brain remodeling after stroke [1,2]. Reactive astrocytes undergo complex context- and time-dependent genetic, morphological, and molecular changes, which are associated with the severity of ischemia and can be regulated by intra- and intercellular signaling pathways [3,4]. In the acute stroke phase, astrocyte reactivity is triggered by alarmins [5] and microglial pro-inflammatory cytokines via the receptor for advanced glycation end products (RAGE) and toll-like receptor 4 (TLR4) [6,7]. The inflammatory response in astrocytes elicits morphological alterations and expression of glial fibrillary acidic protein (GFAP), induces cell proliferation and migration towards the lesion core [3,8-10], and promotes the synthesis of extracellular matrix (ECM) molecules [11–14]. Reactive astrocytes align around the lesion border together with microglia, NG2 cells, and fibroblasts [15,16] to form the glial scar that prevents the spill-over of pro-inflammatory

cytokines and the migration of immune cells into perilesional tissues. Experimental depletion of the glial scar in rodent models of cerebral ischemia increases the infarct size and diminishes functional recovery [8,17,18]. On the other hand, the glial scar inhibits restorative mechanisms after brain injury [19] by inducing inflammation-mediated cell death [20] and neuroplasticity-restricting ECM components [21,22]. Emerging evidence indicates that reactive astrocytes are functionally diverse, and molecular expression analysis identifies neurotoxic "A1" and supportive "A2" phenotypes [1,6]. In the post-acute stroke phase, astrocyte reactivity decreases, and the release of astrocytic growth factors promotes neuroplasticity [23]. As opposed to pro-inflammatory cytokines, astrocytic transforming growth factor beta (TGFβ) limits neuroinflammation during the subacute period after stroke [24]. However, the molecular signals that restrain astrocyte reactivity remain largely unknown.

In the healthy brain, TnC is expressed in stem cell niches and is not produced by mature cells [12,25,26]. In ischemic stroke, TnC has been identified as one of the main components of the fibrotic scar [27] and as an endogenous TLR4 activator [28,29]. Thereby, TnC can regulate astrocyte reactivity and glial scar formation. The *de novo* TnC expression has been reported in the mouse models of retinal ischemia [30] and subarachnoid hemorrhage [31]. In subarachnoid hemorrhage, TnC deficiency reduced brain edema and improved neurological recovery [31]. In retinal ischemia, TnC knock-out ameliorated photoreceptor degeneration [32]. We have recently demonstrated that TnC limits microglial reactivity and immune cell infiltration following transient middle cerebral artery occlusion (MCAO) in mice [33]. The role of TnC in the regulation of post-ischemic astrocytic responses remained unknown. By comparing wild-type (WT) and TnC$^{-/-}$ mice exposed to transient MCAO, we now explored how TnC controls reactive gliosis and astrocyte-microglial interactions. Using high-resolution microscopy and morphological analysis, which we for the first time employed for analysing ischemic tissue, we identified that TnC is an important regulator of astrogliosis.

Results

De novo expression of TnC post-stroke precedes astrogliosis and correlates with astrocyte reactivity

TnC expression in a healthy brain is restricted to neurogenic niches [34]. After stroke, we observed a significant upregulation of TnC in the dorsal part of the ischemic striatum of wild-type animals at 1, 3, 7, and 14 days post ischemia (DPI) (Fig. 1A, C). At 42 DPI, TnC was downregulated back to the control level. The *de novo* expression of TnC strongly correlated ($r = 0.7513$, $p=1.29*10^{-7}$) with reactive astrogliosis detected by GFAP immunolabeling (Fig. 1B, D). Reactive astrocytes were first detected at 3 DPI, indicating that TnC upregulation precedes astrogliosis (Fig. 1E).

TnC deficiency does not alter ischemic lesion size or neurological recovery post-stroke

To evaluate stroke outcomes in WT and TnC$^{-/-}$ mice, we analyzed consecutive brain sections stained with cresyl violet (Nissl) or processed for NeuN immunohistochemistry. We examined animal behavior at 1, 3, 7, 14, and 42 DPI. TnC deficiency did not affect ischemic lesion size, hemispheric swelling in the acute phase, and hemispheric atrophy in the post-acute stroke phase, as shown by Nissl staining (Fig. 2A, B). The density of surviving neurons in the ischemic striatum did not differ between the WT and TnC$^{-/-}$ mice, as shown by NeuN immunohistochemistry (Fig. 2C). Compared with the WT animals, TnC-deficient mice exhibited similar neurological deficits, motor impairment, survival rate, and body weight changes at 1, 3, 7, 14, and 42 DPI (Fig. 2D-G).

Notably, GFAP immunoreactivity was significantly increased in the ischemic striatum of TnC$^{-/-}$ mice at 14 DPI, compared with WT animals (Fig. 1E). At 42 DPI, GFAP expression in TnC$^{-/-}$ mice was lower than in WT animals.

TnC deficiency alters astrocyte morphology in the post-acute stroke phase

Using GFAP immunolabeling, we employed high-resolution confocal microscopy and bias-free automated data analysis to explore the changes in three-dimensional astrocyte morphology in the dorsal part of ischemic striatum, which is the core of the middle cerebral artery territory, in the first six weeks post-stroke (Fig. 3A). Individual reactive astrocytes were detected using the previously established 3DMorph tool [35], which we recently used to characterize post-stroke morphological alterations in microglia [33]. We here successfully used this tool for studying astrocytic responses, which is an important advancement in the field, since previous morphological studies were performed in non-ischemic tissues [36,37].

In line with the increased GFAP immunoreactivity at 14 DPI, the number of reactive astrocytes was significantly higher in TnC$^{-/-}$ mice, compared with the WT animals (Fig. 3B). Segmentation algorithms implemented in 3DMorph provide a vast variety of morphological readouts, which implies careful selection of the meaningful parameters by the user. In our data, the

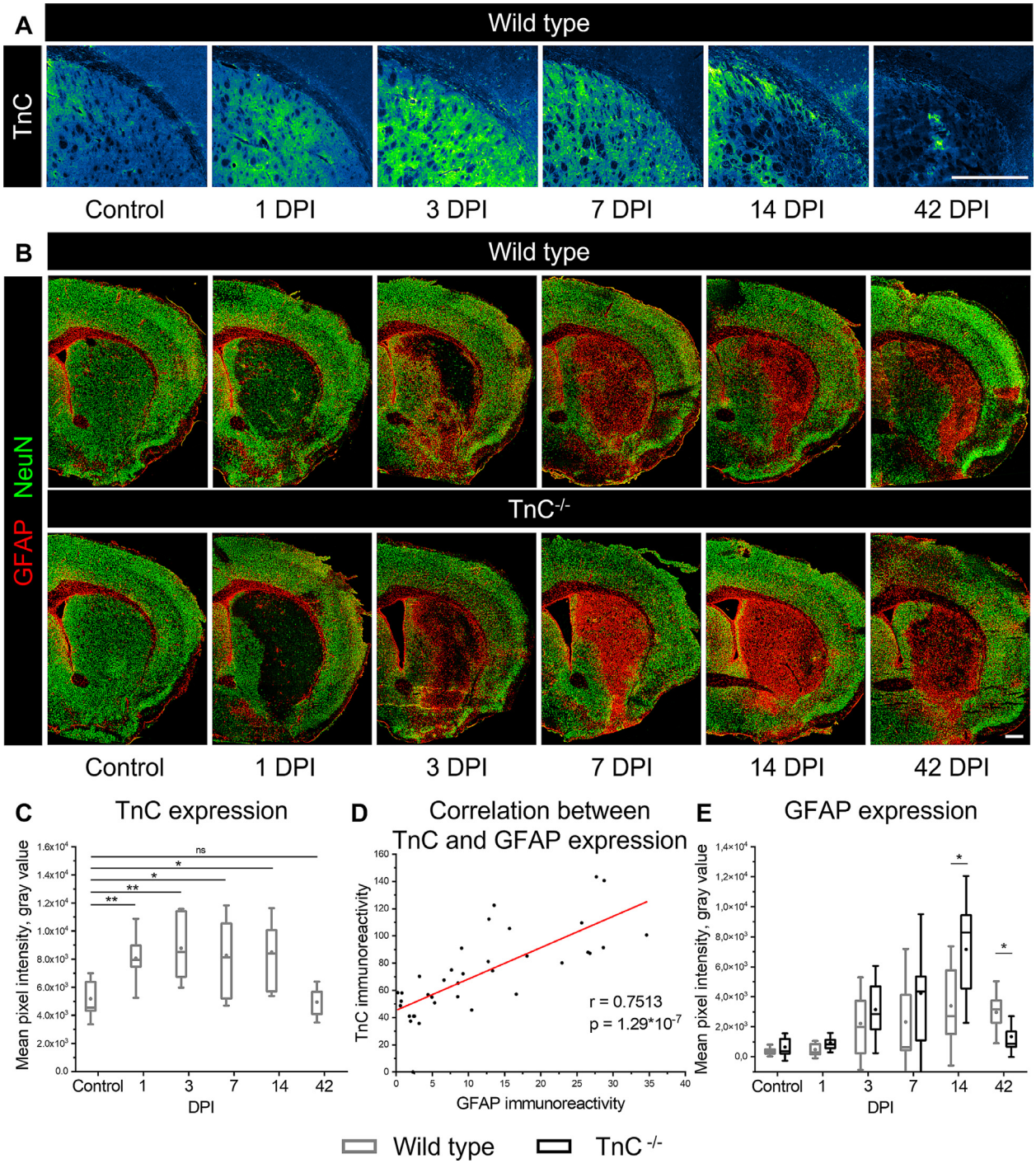

Fig. 1. TnC expression and astrogliosis post-stroke. (A) Representative TnC immunolabeling is shown in the dorsal part of the ischemic striatum of wild-type control mice and at 1, 3, 7, 14, and 42 DPI. (B) Representative immunolabeling of reactive astrocytes (GFAP, red) is shown in the ischemic striatum of wild type and TnC$^{-/-}$ mice at 1, 3, 7, 14, and 42 DPI. Neuronal labeling (NeuN, green) is shown to visualize the ischemic lesion borders. (C) TnC expression is quantified in the dorsal part of the ischemic striatum of wild-type mice at 1, 3, 7, 14, and 42 DPI. (D) The plot shows a linear correlation between TnC and GFAP immunoreactivity. (E) GFAP expression is quantified in the dorsal part of the ischemic striatum of wild type and TnC$^{-/-}$ mice at 1, 3, 7, 14, and 42 DPI. In control animals, no stroke was induced. Scale bars, 500 μm. DPI, days post ischemia. Boxes are 25-75% IQR, circles are means, lines are medians, whiskers are SD. Asterisks denote significant differences between genotypes as indicated by Kruskal-Wallis and Mann-Whitney tests (*$p<0.05$, **$p<0.01$, ***$p<0.001$), n=9.

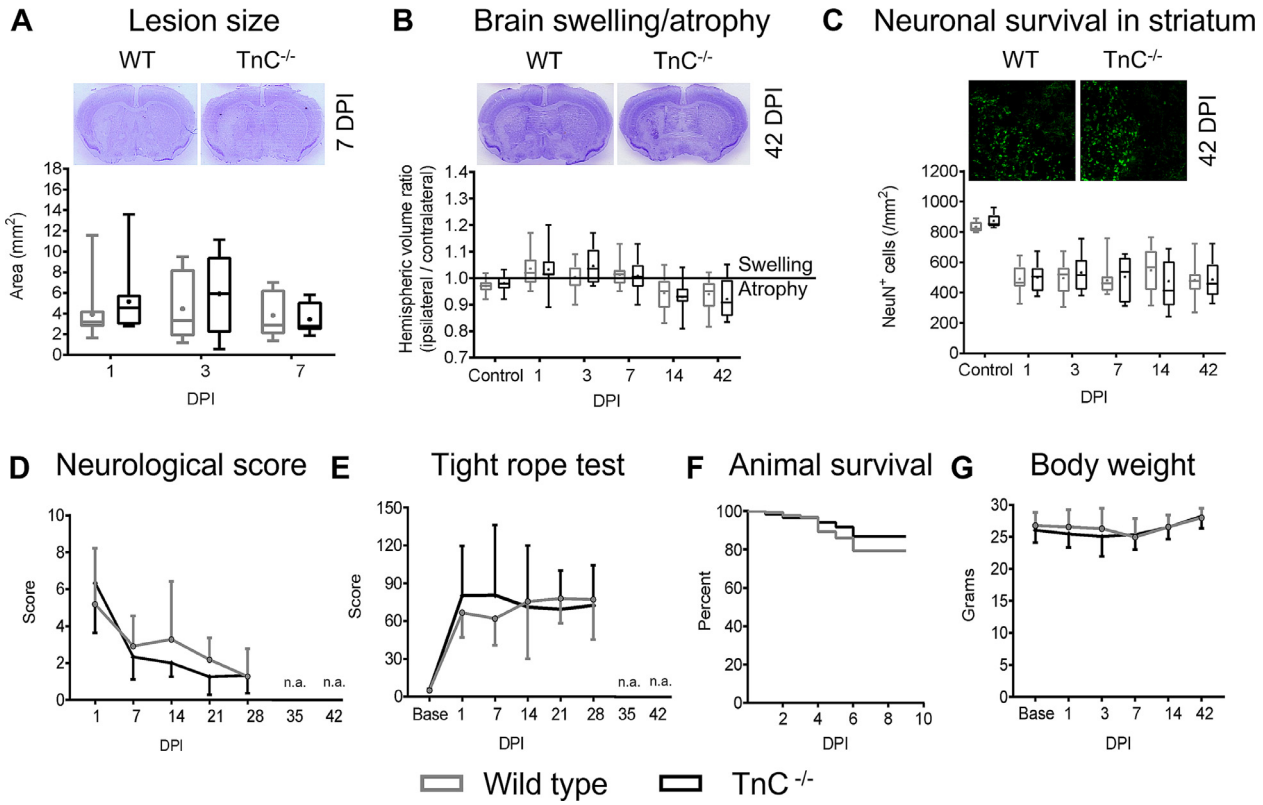

Fig. 2. TnC deficiency does not affect stroke outcomes in the acute and post-acute phase. (A) Lesion size quantified as the area of the brain section (bregma level) that is devoid of Nissl staining. (B) Hemispheric volume ratio (ipsilateral/contralateral to the ischemic lesion) quantifications indicate brain swelling (values >1) and atrophy (<1). (C) Neuronal density in ischemic striatum. (D) Neurological score. (E) Tight rope test score. (F) Animal survival. (G) Body weight. In control animals, no stroke was induced. DPI, days post-ischemia. n.a., not assessed. Data in (A-C) are box plots with boxes as 25-75% IQR, circles are means, lines are medians, whiskers are minimum and maximum values. Data in (D-G) means ± SD. No differences between genotypes were detected by two-way ANOVA and Fisher's LSD tests, n=11.

following parameters contributed to at least 97% of the intra-group variance in all samples: branch length, number of branching points, and territorial volume. Therefore, further analysis was focused on these three parameters. The territorial volume of individual astrocytes, which was approximated as volume of the circumscribed polyhedrons, increased at 3 DPI in both genotypes [WT: 12±5 (1 DPI) vs 32±3 (3 DPI), p=0.034; $TnC^{-/-}$: 16±3 (1 DPI) vs 31±2 (3 DPI), p=0.001; data are mean±s.e.m in thousands μm^3]. Together with increased branch length [WT: 6.9±1.5 (1 DPI) vs 10±0.5 (3 DPI), p=0.033; $TnC^{-/-}$: 7.9±0.8 (1 DPI) vs 11.9±0.4 (3 DPI), p=0.0004; data are mean±s.e.m in μm], these data indicate astrocytic hypertrophy that evolves in the acute phase.

In comparison with the WT, territorial volume was moderately but significantly decreased in $TnC^{-/-}$ animals at 14 and 42 DPI (Fig. 3C). The average branch length and the number of branching points (Fig. 3D, E) were also significantly reduced in $TnC^{-/-}$ mice, indicating that TnC deficiency makes reactive astrocytes more compact.

Because the distribution of morphological parameters of reactive astrocytes was bimodal at 42 DPI, we further segregated their phenotypes into the compact and ramified subtypes using hierarchical cluster analysis (Fig. 4A). Territorial volume, branch length and number of branching points per cell were significantly different ($p<0.01$, two-sample t-test) between the compact and ramified astrocytes in both WT and $TnC^{-/-}$ genotypes. While the proportions of the clusters were similar in WT and $TnC^{-/-}$ genotypes (Fig. 4B), TnC deficiency reduced territorial volume, average branch length, and number of branching points in both compact and ramified cells, making the difference between these subtypes less evident (Fig. 4C-E).

TnC deficiency increases aggrecan expression in the post-acute stroke phase

As a multifunctional glycoprotein, TnC has multiple interaction partners [38], and its absence can affect the expression of other ECM components in

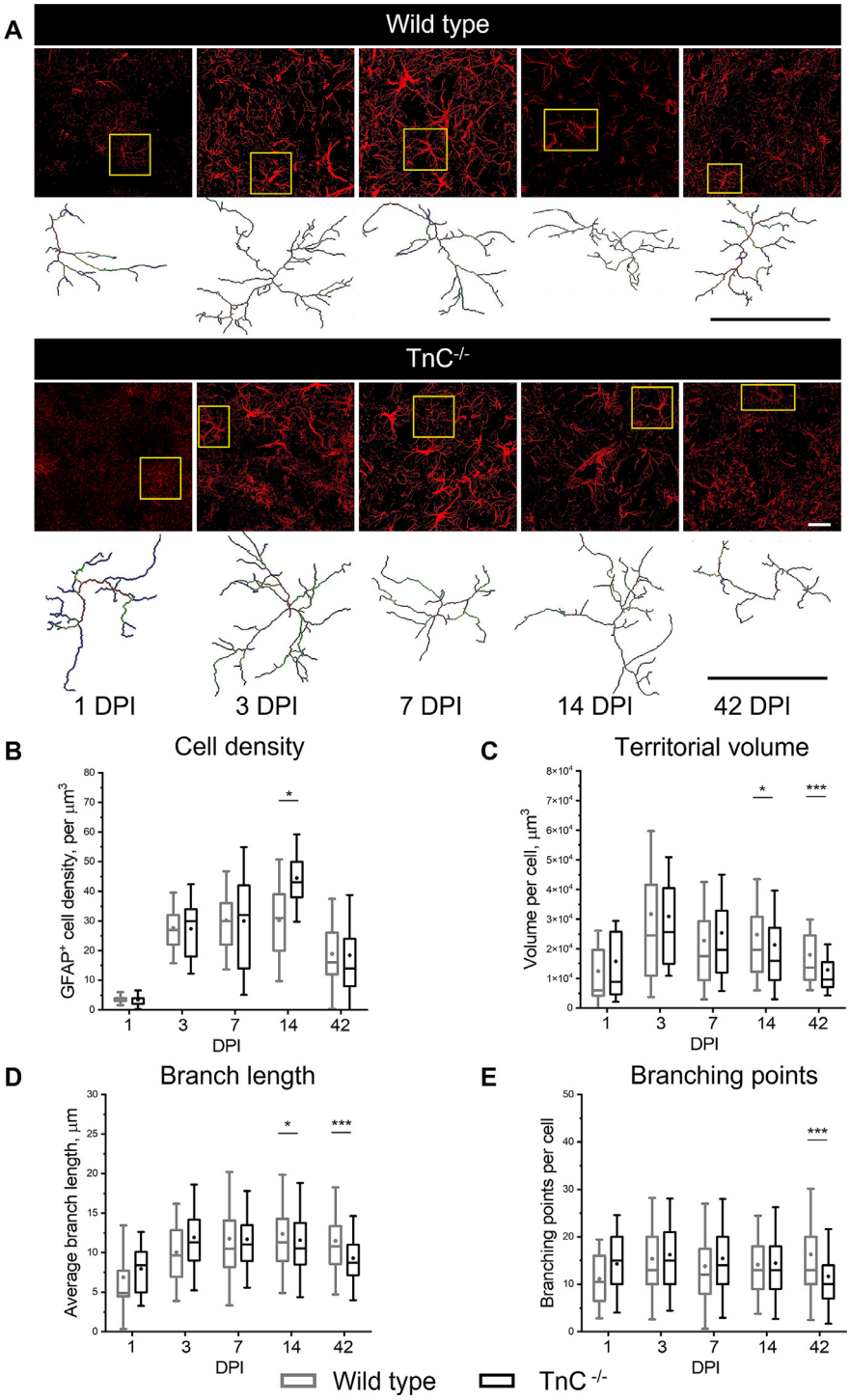

Fig. 3. Three-dimensional morphology of reactive astrocytes after stroke. (A) Representative confocal images (z-projections) show reactive astrocytes (GFAP, red) and the corresponding reconstructions of their three-dimensional morphology in the dorsal part of the ischemic striatum of WT and $TnC^{-/-}$ mice at 1, 3, 7, 14 and 42 DPI. Scale bars, 25 μm. (B-E) Morphological analyses evaluating reactive astrocyte cell density (B), territorial volume (C), branch length (D), and number of branching points (E) are shown for WT and $TnC^{-/-}$ mice at 1, 3, 7, 14 and 42 DPI. In control animals, no stroke was induced. DPI, days post ischemia. Boxes are 25-75% IQR, circles are means, lines are medians, whiskers are minimum and maximum data. Asterisks denote significant differences between genotypes as indicated by Kruskal-Wallis and Mann-Whitney tests (*$p<0.05$, ***$p<0.001$), n=9.

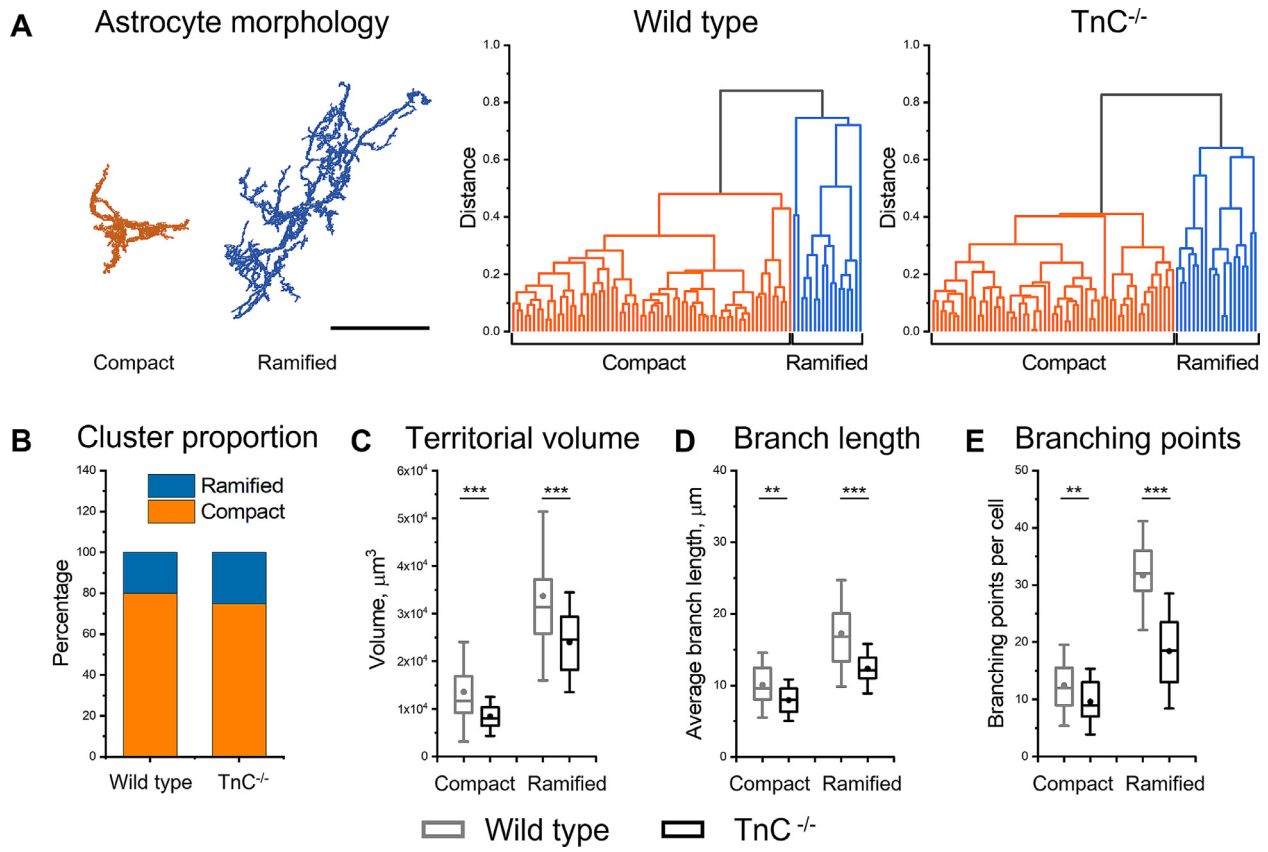

Fig. 4. Classification of reactive astrocyte morphology subtypes at 42 DPI. (A) Hierarchical cluster analysis detects the compact and ramified subtypes of reactive astrocytes. Scale bar, 25 µm. (B-E) The compact and ramified astrocytes are separately quantified, showing cluster proportions (B), territorial volume (C), average branch length (D), and the number of branching points (E) in the dorsal part of the ischemic striatum of WT and TnC$^{-/-}$ mice at 42 DPI. DPI, days post-ischemia. Boxes in box plots are 25-75% IQR, circles are means, lines are medians, whiskers are SD. Asterisks denote significant differences between genotypes as indicated by Mann-Whitney tests (*p<0.05), n=9.

the ischemic brain. Here, we examined the expression of the two major ECM proteoglycans, brevican and aggrecan, in the ischemic striatum of WT and TnC$^{-/-}$ mice at 42 DPI by Western blot (Fig. 5A). Both brevican and aggrecan are chondroitin sulfate proteoglycans that modulate neuronal plasticity [39,40]. While brevican is commonly associated with astrocytes [41], aggrecan contributes to perineuronal matrix formation and restricts axonal outgrowth [42]. TnC deficiency did not affect brevican expression but induced an upregulation of aggrecan at 42 DPI (Fig. 5B).

TnC deficiency alters astrocyte-microglial interaction

Reactive astrocytes and microglia vividly interact during neuroinflammation in neurodegenerative diseases and stroke [43,44]. To evaluate the role of TnC in astrocyte-microglial interaction, we co-cultivated primary astrocytes and microglia obtained from WT and TnC$^{-/-}$ mice in all four possible combinations. After 3 to 7 days *in vitro*, astrocytic cultures form monolayers and exhibit high expression of GFAP, resembling reactive astrocytes after brain injury [45,46]. The migration of microglia on astrocytic monolayers was quantified using time-lapse microscopy and cell tracking (Fig. 6A and Supplementary Video 1). Cell types were identified at the end of live-cell imaging experiments by astrocytic GFAP and microglial marker protein Iba1 immunolabeling. TnC deficiency significantly reduced both average and maximum microglial migration speed (Fig. 6B, C). Although the lowest migration speed was observed in TnC$^{-/-}$/WT and TnC$^{-/-}$/ TnC$^{-/-}$ astrocyte/microglia combinations, TnC$^{-/-}$ microglia also migrated slower on WT astrocytes. In TnC$^{-/-}$ microglia, the expression of intercellular adhesion molecule 1 (ICAM1) was significantly higher than in WT, as indicated by immunolabeling quantifications (Fig. 6D, E).

In TnC$^{-/-}$ mice, the expression of ICAM1 overlapping with Iba1 staining was significantly higher than

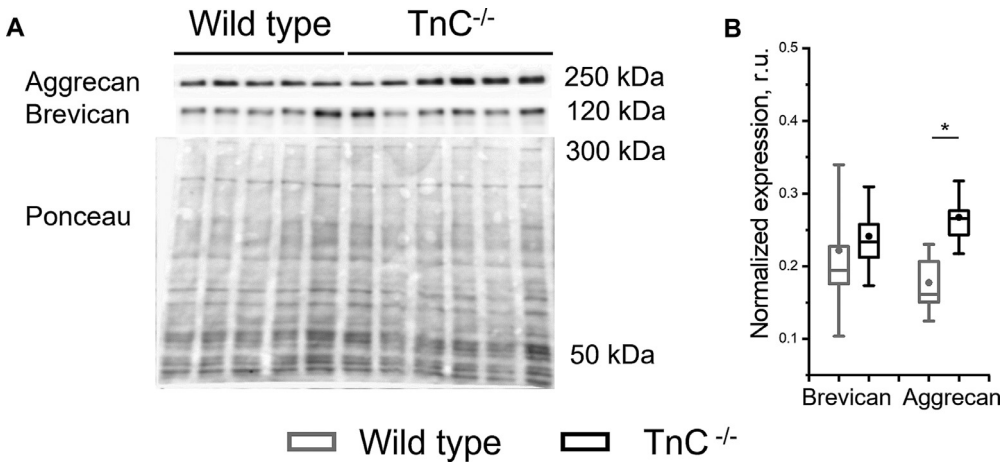

Fig. 5. Protein expression of aggrecan and brevican at 42 DPI. (A) The representative Western blot shows the expression of aggrecan (approx. 250 kDa bands) and brevican (approx. 120 kDa bands) in the ischemic striatum of WT and TnC$^{-/-}$ mice at 42 DPI. We used Ponceau staining as a loading control (multiple bands 300-25 kDa). Each vertical line corresponds to one animal. Normalized protein expression of brevican and aggrecan is shown in (B). Boxes in box plots are 25-75% IQR, circles are means, lines are medians, whiskers are minimum and maximum data. Asterisks denote significant differences between genotypes as indicated by Mann-Whitney tests (*p<0.05), n=5.

in WT mice at 1 and 7 DPI (Fig. 6F, G), which confirms the results obtained *in vitro*.

Discussion

Cellular responses in glia and ECM reorganization are essential for brain remodeling after stroke. While ample evidence indicates that reactive astrocytes restrict secondary damage associated with inflammatory signaling in ischemic lesions, ECM remodeling and astrocyte-ECM interactions post stroke remain under investigated. Damage-associated molecular patterns were shown to induce astrocyte reactivity, while the molecules that restrain astrogliosis were largely unknown. Here, we examined how astrocytic responses are influenced by TnC$^{-/-}$ during the first six weeks after stroke. Using high-resolution microscopy and cutting-edge image analysis methods, we demonstrate that the *de novo* expression of TnC by reactive astrocytes acts as a homeostatic regulator restricting excessive astrogliosis.

Ischemic brain injury and stroke recovery

Our results revealed that the severity and dynamics of post-stroke brain swelling/atrophy and neurological recovery are similar in WT and TnC$^{-/-}$ mice, indicating that TnC deficiency does not exacerbate ischemic injury, which is consistent with our previous observations [33]. In this study, lesion size, brain edema/ atrophy and neuronal density did not change significantly over time post ischemia, which is different from previous studies in photothrombotic stroke [47,48] and neonatal hypoxia [49]. Lesion size, brain edema/ atrophy and neuronal density were not influenced by TnC$^{-/-}$, indicating that TnC deficiency did not induce neuroprotection. However, TnC may play a more prominent role for neuronal survival under conditions of more slowly evolving neuronal degeneration, e.g., in chronic neurodegenerative diseases. Further studies will be required to elucidate this issue.

De novo expression of TnC in reactive astrocytes

In the healthy brain, TnC is expressed in neurogenic niches [34,38,50] and contributes to cell proliferation and differentiation control. Although TnC is not produced by terminally differentiated brain cells, we have recently shown that this glycoprotein is abundantly expressed in the ischemic striatum after stroke [33]. Here, we demonstrate that the *de novo* expression of TnC reaches its maximum at 3 DPI, remains upregulated during the post-acute stroke phase, and fades away in the chronic phase. These results are consistent with previous studies showing TnC upregulation shortly after brain injury [51,52].

In WT mice, TnC expression positively correlated with GFAP expression in all timepoints, indicating that reactive astrocytes are the major source of TnC in the ischemic brain tissue. Also, TnC is one of the most abundant ECM proteins secreted by astrocytes after brain injuries that are not related to stroke [12,27]. Conclusively, the *de novo* expression of TnC is a typical hallmark of reactive gliosis, regardless of the brain injury origin. Unlike WT cells, reactive TnC$^{-/-}$ astrocytes were not able to synthesize TnC, and reactive gliosis was significantly increased in TnC$^{-/-}$ mice at 14 DPI. The impact of TnC

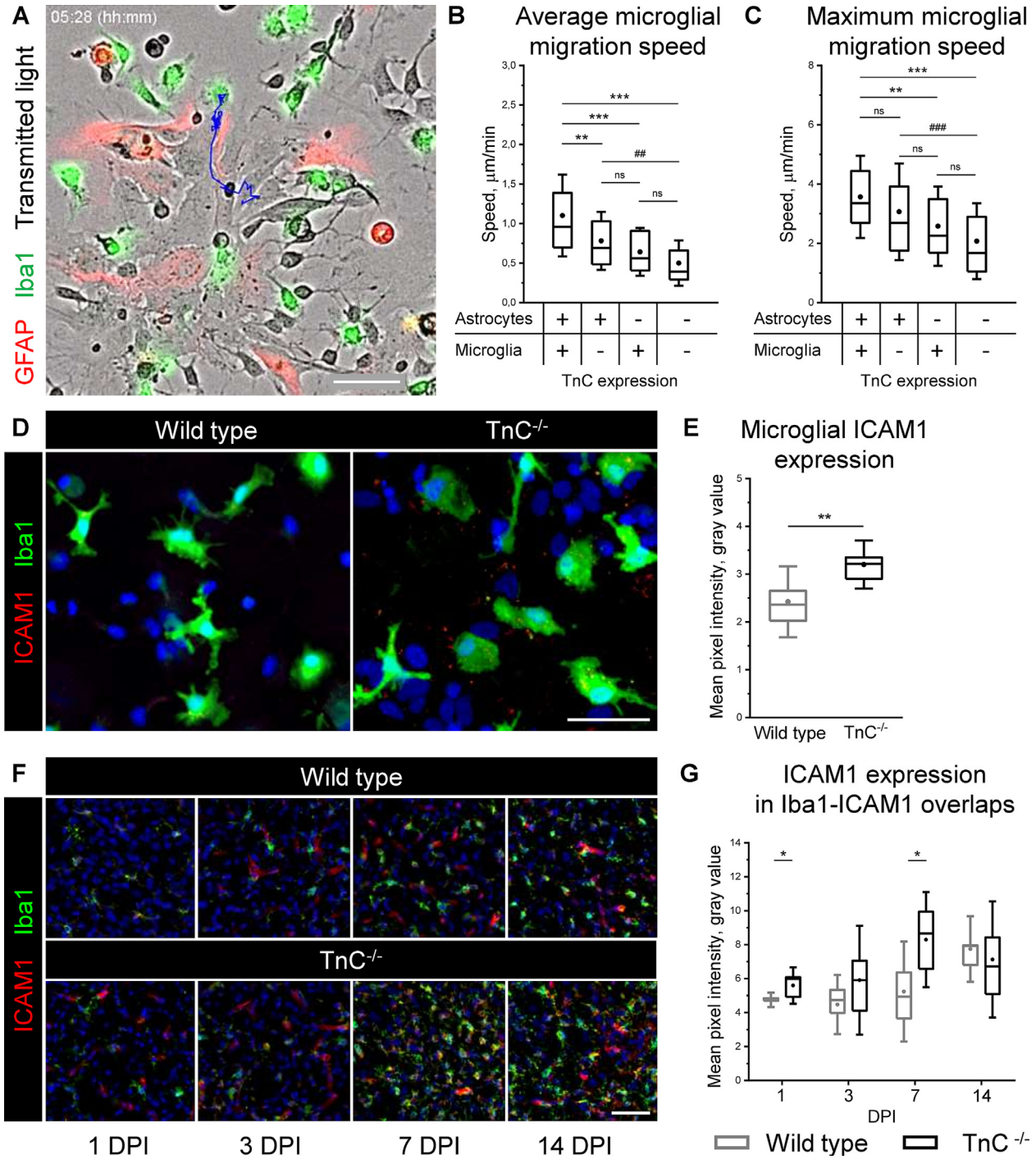

Fig. 6. Microglial migration and adhesion. (A) Live cell imaging and microglia cell tracking in astrocyte-microglial co-cultures. A single microglia migration track during the 328-minute imaging period is shown in blue. Cell types were identified by GFAP (red) and Iba1 (green) immunolabeling at the end of the time-lapse imaging shown in Supplementary Video 1. Average (B) and maximum (C) microglia migration speed are quantified in astrocyte-microglial co-cultures obtained from WT and TnC$^{-/-}$ mice, in all four combinations. (D) Representative immunolabeling of ICAM1 (red) and Iba1 (green). (E) Microglial ICAM1 immunolabeling intensity. (F) Representative immunolabeling of ICAM1 (red) and Iba1 (green) is shown in the dorsal part of the ischemic striatum of WT and TnC$^{-/-}$ mice at 1, 3, 7, and 14 DPI. (G) ICAM1 immunolabeling overlapping with Iba1 staining is quantified in the dorsal part of the ischemic striatum of WT and TnC$^{-/-}$ mice at 1, 3, 7, and 14 DPI. Scale bars, 50 µm. DPI, days post ischemia. Boxes are 25-75% IQR, circles are means, lines are medians, whiskers are SD. Asterisks and hashes denote significant differences between genotypes as indicated by Kruskal-Wallis and Mann-Whitney tests in (G) (*$p<0.05$), n=5, and t-tests in (B, C, and E) (**$p<0.01$, ***$p<0.001$, $^{\#\#}p<0.01$, $^{\#\#\#}p<0.001$), 60 cells per condition, n=3.

deficiency accumulated throughout the acute phase post stroke and resulted in increased cell density and reduced territorial volume of reactive astrocytes in the ischemic striatum at 14 DPI. In the chronic stroke phase at 42 DPI, astrocytic morphology alterations were even more pronounced, as indicated by the reduced territorial volume and branching. Since TnC is predominantly produced by reactive astrocytes, we hypothesize that TnC acts as a homeostatic regulator of reactive gliosis. That is, the release of TnC by reactive astrocytes can attenuate astrogliosis. Our observations are coherent with the previous *in vivo* research indicating exacerbated astrogliosis in TnC-deficient mice [53], and the *in vitro* studies reporting that TnC supports the quiescent state in cultivated human astrocytes [54].

TnC and its binding partners in the extracellular matrix

TnC is a multifunctional glycoprotein that contains a C-terminal fibrinogen-related domain, recurrent fibronectin and epidermal growth factor (EGF) domains, and heptad repeats [38]. Due to the heptad repeats at the N-terminus, TnC can form hexamers, and was formerly known as hexabrachion [55,56]. Because of the modular structure, TnC interacts with multiple ECM molecules including fibronectin [57], integrins [58], and chondroitin sulfate proteoglycans (CSPGs) [59]. The interplay of fibronectin and TnC promotes the expression of metalloproteinases that can degrade ECM [60], but the binding between TnC and CSPGs may stabilize ECM complexes. CSPGs restrict neuroplasticity after stroke [61,62], and in this work we observed increased expression of aggrecan, one the major CSPGs in the brain, at 42 DPI in $TnC^{-/-}$ mice. We hypothesize that the upregulation of aggrecan inhibits post-stroke neuroplasticity, which could explain the fact that $TnC^{-/-}$ animals did not show better neurological recovery than WT mice.

TnC is a homeostatic regulator of glial morphology

Reactive astrocytes are commonly identified by their hypertrophic morphology [23]. In this study, we combined high resolution microscopy and cutting-edge image processing methods to provide an in-depth evaluation of three-dimensional astrocytic morphology in ischemic tissue in the acute, post-acute, and chronic stroke phase. *De novo* expression of TnC preceded reactive astrogliosis in the acute stroke phase and TnC deficiency resulted in altered astrocytic morphology in the post-acute and chronic stroke phases.

In the post-acute stroke phase, reactive astrocytes segregated into the compact and ramified phenotypes. In contrast to the compact subtype, ramified astrocytes had longer, arborized branches and larger cell territories. Previously, a similar phenotype of reactive astrocytes with high GFAP expression and elongated processes has been described in a rat model of ischemic stroke using manual morphological analysis [63]. $TnC^{-/-}$ astrocytes were more compact than WT astrocytes, as evidenced by the reduced territorial volume, branch length and number of branching points. Of note, the differences between genotypes were especially pronounced for the ramified subtype. This finding indicates that TnC produced by reactive astrocytes favors their ramification. In line with the recent evidence showing functional diversity of reactive astrocytes [6,64], the ramified phenotype likely represents the supportive regulatory astrocytes. Earlier [33], we demonstrated that TnC supports the ramification of activated microglia after stroke. Here, we report the similar influence on reactive astrocytes, which designates TnC as a general regulator of reactive glia morphology.

On the molecular level, this regulatory function of TnC can be associated with the activation of TLR4 and RAGE receptors on the surface of glial cells [28,65,66]. However, the exact molecular mechanism by which TnC promotes ramification of reactive glia remains to be resolved.

TnC regulates astrocyte-microglial interactions

The induction of astrocytic reactivity by pro-inflammatory cytokines released from activated microglia is a key mechanism of neuroinflammation in neurological diseases including stroke [2,6,44,67]. Here, we observed that TnC deficiency impairs microglial migration on the astrocytic surface. Therefore, activated microglia spend more time in contact with $TnC^{-/-}$ astrocytes. We suggest that the prolonged interaction between astrocytes and microglia promotes stronger astrocytic responses, which is supported by morphological alterations in $TnC^{-/-}$ astrocytes reported in this study. The increased astrocyte-microglial adhesion is likely mediated by the upregulation of ICAM1 associated with $TnC^{-/-}$ microglia that we observed both *in vitro* and *in vivo*. The role of ICAM1 in post-stroke neuroinflammation is commonly attributed to the increased adhesion between peripheral blood leukocytes and brain vascular endothelium [68,69] mediated by integrin $\alpha L\beta 2$ [70], also known as leukocyte function associated antigen 1 (LFA-1). To the best of our knowledge, the involvement of ICAM1 in astrocyte-microglial adhesion has not been reported. However, ICAM1 binds the $\beta 3$ integrin subunit [71], which is part of the astrocytic $\alpha V\beta 3$ integrin complex involved in reactive gliosis [72]. Thus, our data suggests that TnC restricts post-ischemic astrogliosis by inhibiting ICAM1-mediated astrocyte-microglial interaction.

Strengths and limitations

This study identified TnC as a negative regulator of post-ischemic astrogliosis, which maintains astrocytic territorial volume, branching point number, and branch length. Automated analysis for the first time allowed to evaluate astrocytic morphology in previously ischemic brain tissue. Large sample sizes in combination with strict examiner blinding eliminated data bias. The analysis of astrocytic morphology was based on GFAP immunolabeling, which makes our results applicable within the conditions involving reactive gliosis. For extending the applicability of our method, the markers of quiescent astrocytes or genetically encoded reporters can be used. Although the comparison of WT and TnC$^{-/-}$ genotypes suggests causative links between TnC expression and astrocytic phenotypes, this study was descriptive in nature and observations on the interactions of TnC and astrocytes are based on correlations. The analysis of microglial migration on the surface of astrocytes provided evidence for the involvement of TnC in astrocyte-microglial interaction *in vitro*. The implemented co-cultivation approach is reductionistic in nature and requires considering more complex multicellular interactions in subsequent *in vivo* experiments. Future studies should further explore the molecular mechanisms via which TnC regulates astrocyte-microglial interactions and restricts post-ischemic astrogliosis. Such studies may point out targets for neurorestorative stroke therapy.

Conclusion

Reactive astrocytes produce TnC to restrict excessive gliosis and to maintain the ramified presumably supportive regulatory astrocytic phenotype.

Experimental procedures

Animals

117 wild-type (WT) and 110 transgenic TnC$^{-/-}$ male 129/Sv mice (8-12 weeks, 23-28 g) were employed in this study [73]. 7 WT and 8 TnC$^{-/-}$ male and female 129/Sv mice (newborns, postnatal day 1 and 2) were used for preparing cell cultures. The genotypes were determined by PCR followed by electrophoresis in 2% agarose gel. The following primers were used: tnc_low (ttctgcaggttggaggcaac), tnc_up (ctgccaggcatctttctagc) and tnc_neoup (ctgctctttactgaaggctc). Animals were housed in groups of 3-5 mice per cage in a 12h:12h human light/dark cycle. Food and water were provided *ab libitum*. All experimental procedures were approved by the local ethical committee (Bezirksregierung Düsseldorf; project G4585/16) and were performed in compliance with ARRIVE guidelines (Animal Research Reporting of In Vivo Experiments) and E. U. guidelines (Directive 2010/63/EU) for the Care and Use of Laboratory Animals.

Experimental design

Focal cerebral ischemia was induced by transient MCAO in WT and TnC$^{-/-}$ mice. Animals were randomly assigned into groups using a customized R script (see Supplement 1). Histochemical and cell morphology analyses were performed at 1, 3, 7, 14, and 42 days post-ischemia (DPI). Behavioral tests were performed at 1, 7, 14, 21, and 28 DPI in the long-term assessment group that survived until 42 DPI. Tissues for Western blot analysis were obtained from 42 DPI mice. In all experiments, naive animals of both genotypes were used as control group.

Middle cerebral artery occlusion (MCAO)

Intraluminal transient MCAO was induced for 35 min which results in moderate-sized focal lesions encompassing the striatum allowing long-term animal survival [33]. The MCAO procedure is explained in detail in the Supplement 2. We provided postoperative care by injecting carprofen (4 mg/kg in 500 μl Ringer solution) daily during the first week post-ischemia. Feeding was facilitated by moistened food. Mice were weighed daily. Animals exhibiting body weight loss $>$20% of baseline were excluded, as stated in the approved animal proposal (Landesamt für Umwelt und Verbraucherschutz (LANUV) Recklinghausen; project G4585/16).

Behavioral testing

Neurological deficits and motor impairments were evaluated at 1, 7, 14, 21, and 28 DPI. We assessed general and focal neurological deficits using Clark's neurological score [74]. Animal behavior was observed in an open bench or during the tail suspension, as described in the Supplement 3. Motor coordination deficits were analyzed with the tight rope test using a 60 cm long rope that connects two platforms at the height of 50 cm. The time to grasp, time to reach, and circling behavior were included in the score evaluation. The maximum duration of the test was 60 s, and in all cases, the test was repeated six times. The scores were calculated using the customized R script.

Nissl staining and volumetry

We performed cresyl violet (Nissl) staining to evaluate hemispheric swelling/atrophy. At defined time

points, mice were sacrificed under deep isoflurane anesthesia by transcardial perfusion with 20 ml of 0.9% ice-cooled saline, followed by 20 ml of 4% v/v paraformaldehyde (PFA) in 0.1 M tris buffer saline, pH 7.2 - 7.4 (TBS). The brains were carefully harvested from the skull and post-fixed overnight in 12 ml of 4% PFA. Next, brain cryoprotection was achieved by sequential immersion in 12 ml of 15% and 30% sucrose until sinking. Finally, the brains were frozen in dry ice and stored at -80 °C for further processing.

Coronal cryosections (30 μm thick) were collected on cold microscope slides (ThermoFisher Scientific, Cat# J1800AMNT). Sequential sections (12 sections, 500 μm interval) across the forebrain were stained with cresyl violet solution (see Supplement 4 for details) and scanned (1200 × 1200 PPP, 24 bits). To determine hemispheric swelling/atrophy, we measured ischemic (ipsilateral) and non-ischemic (contralateral) hemispheric areas in each section using the *freehand* and *measure* tools in FIJI. The hemispheric volumes (H_v) were calculated as $H_v=\sum A_S*T*I$, were A_S is hemispheric area measured in a section, T is the section thickness, and I is the interval between sections. Ischemic lesion size was evaluated by measuring the infarct area by manually delineating the region devoid of cresyl violet staining in the cryosections at the bregma level at 1, 3, and 7 DPI.

Cell cultures

Primary astrocytic and microglial cultures were obtained by dissociating the cortices of newborn mice as described previously [45], with minor modifications. In brief, dissociated cortical cell suspensions were plated onto cell culture flasks coated with poly-D-lysine (PDL) and maintained for expansion in glia-selective medium (DMEM with 10% fetal bovine serum 4,5 g/l glucose, supplemented with L-glutamine) for 7 days at 5% CO_2 and 37 °C. Microglia cells were removed by shaking on a rotary shaker (150 rpm for 1 h) and cultivated separately for 5 days. The remaining mixed cultures containing astrocytes, NG2 glia, and residual microglia were treated with 20 μM cytosine-1-β-D-arabinofuranoside (AraC) for 2 days and the cell debris was removed by shaking to obtain pure astrocytes. Astrocytes were sub-cultivated in PDL-coated 96-well plates (μ-Plate 96 well black, Cat# 89626, Ibidi, Gräfelfing, Germany), 50000 cells per well, and incubated for 3 days to form monolayer cultures. Microglia were seeded (30000 cells per well) onto the astrocytic monolayers and allowed to settle for 3 h before live cell imaging. Microglia and astrocytes obtained from $TnC^{-/-}$ and WT mice were co-cultivated in all four possible combinations.

Live cell imaging and microglia migration tracking

Astrocyte-microglial co-cultures were monitored for 6 h using the fully automated ImageXPress Pico imaging system (Molecular Devices, San Jose, USA). Every 4 min, the snapshots of 1387 × 1387 μm regions of interest (10x/0.32 objective) positioned in the center of each well were obtained using the transmitted light imaging mode. At the end of live cell imaging experiment, cell cultures were fixed with 4% PFA for 15 min and processed for GFAP, Iba1, and ICAM1 immunocytochemistry. Thereby, astrocytes and microglia were identified in the same regions of interest as recorded during the previous time-lapse imaging. Individual microglia cell migration tracks were analyzed using the standard manual tracking FIJI tool.

Immunolabeling procedures

PFA-fixed brain sections from the level of bregma +0.98 to +0.56 mm were processed for immunohistochemistry as described in the Supplement 5. Primary antibodies detecting neurons (chicken anti-NeuN; 1:300; Millipore Cat# ABN91, RRID: AB_11205760), astrocytes (rat anti-GFAP; 1:300; Thermo Fisher Scientific Cat# 13-0300, RRID: AB_2532994), microglia (rabbit anti-Iba1; 1:500; Wako Cat# 019-19741; RRID:AB_839504), ICAM1 (mouse anti-ICAM1; 1:500; R&D Systems, Cat#AF796; RRID:AB_2248703) and TnC (rabbit anti-TnC; 1:250; Kaf-15, from [75]) were used in combination with secondary antibodies conjugated to Alexa 488, 594, and 647 fluorophores.

Wide field microscopy and quantification of immunofluorescence

The AxioObserver Z1 epifluorescence microscope (objective Plan-Apochromat 10x/0.45 M25; Zeiss, Jena, Germany) was used for imaging the entire ischemic hemisphere by tiling and stitching the adjacent fields of view. The scanning parameters and the FIJI script for image pre-processing are provided in Supplement 6. Neuronal density was estimated in the dorsal striatum by quantifying the $NeuN^+$ cells using the standard *particle analysis* tool for FIJI (size=40-100; circularity=0.50-1.00). Cell density was calculated as the ratio between the cell number and the area of the striatum. TnC immunoreactivity was analyzed by measuring the mean pixel fluorescence intensity in the 2048 × 1620 μm regions of interest positioned within the dorsal striatum. Microglia-associated ICAM1 expression was analyzed in the 2048 × 1620 μm regions of interest positioned within the dorsal striatum by measuring the mean pixel fluorescence intensity within the Iba1

staining binary masks generated by automatic Otsu thresholding algorithm using the standard FIJI tools.

Confocal microscopy and morphological analysis

Three-dimensional morphology of astrocytes was analyzed via GFAP immunolabeling. High-resolution confocal microscopy was performed in representative regions positioned within the estimated core of ischemic lesion. For each brain Section 184.52 $\times$ 184.52 $\times$ 15 μm z-stacks (pixel size 180 nm, slice separation 500 nm) were scanned using the Leica TCS SP8 confocal microscope (63x HC PL APO CS2 objective; Leica, Wetzlar, Germany). Immunolabeling artifacts were eliminated by pre-processing as specified in the Supplement 7.

Individual astrocytes were detected using the 3DMorph [35] processing pipeline for MATLAB (MathWorks, RRID: SCR_001622), and their three-dimensional morphology was analyzed with segmentation algorithms, as described in the Supplement 8. Key morphological parameters were defined based on their cumulative contribution to intra-group variance. The ramified and the compact astrocyte subtypes were detected by hierarchical cluster analysis using the group average method. Distance type was Euclidean, variables were normalized to [0,1], number of clusters was 2, cluster centers were not pre-defined. Differences between cluster means were verified by two-sample t-tests. No clusters were assigned if the mean values were not significantly different between clusters for more than one morphological parameter.

For quantifying microglial ICAM1 expression in primary cell cultures, low-resolution confocal microscopy (20x Plan-Apochromat objective, pixel size 230 nm) was performed in representative regions of interest (236 $\times$ 236 $\times$ 5 μm). ICAM1 expression was analyzed by measuring the mean pixel fluorescence intensity within the Iba1 staining binary masks generated by automatic Otsu thresholding algorithm using the standard FIJI tools.

Protein isolation and Western blots

Western blots were performed to evaluate the differences in the expression of two major ECM proteoglycans, brevican and aggrecan, between WT and $TnC^{-/-}$ genotypes at 42 DPI. Mice were sacrificed under deep isoflurane anesthesia by transcardial perfusion with 20 ml ice-cooled 0.9% saline. The brains were harvested from the skull, and the ischemic striatum was carefully dissected, homogenized, and quickly frozen on dry ice. Total protein extraction, SDS-PAGE electrophoresis, protein transfer and immunodetection were performed as described in the Supplement 9.

Statistical analysis

Data analysis was conducted using GraphPad Prism version 8.0.2 (RRID:SCR_002798) and OriginPro (RRID:SCR_014212) for Windows. Animal survival was analyzed using the Long-rank (Mantel-Cox) test. Body weight was analyzed using repeated measurements two-way analysis of variance (RM-ANOVA, Mixed-effects test). Lesion size, brain atrophy, neuronal survival, TnC immunoreactivity and GFAP expression data were analyzed by two-way ANOVA. Uncorrected Fisher's LSD test for multiple comparisons was applied for exploring the differences between WT and $TnC^{-/-}$ genotypes at each time point. Microglia cell migration and ICAM1 expression *in vitro* were analyzed by one-way ANOVA and pairwise t-tests, Bonferroni correction was applied for multiple comparisons. Normality of data distribution was evaluated by Kolmogorov-Smirnov and Shapiro-Wilk tests. Due to their non-normal distribution, morphological analyses and Western blots were evaluated by Kruskal-Wallis tests, and the Bonferroni correction was applied for multiple comparisons. Pairwise comparisons were performed using Mann-Whitney tests. In all experiments, the significance level was set as α=0.05, and the $p<0.05$ values indicated significant differences between groups.

Author contribution statement

Conceptualization, Funding acquisition, Resources, Supervision, Writing - review & editing: DMH and AF Data curation, Formal analysis, Investigation, Methodology, Validation, Visualization, Writing - original draft, Writing - review & editing: ED and DM-C Methodology, Validation, Writing - review & editing: JR Investigation, Methodology, Visualization, Writing - review & editing: PV and MPE. DMH and AF designed the study. DM-C, PV, MPE, JR and ED performed experiments and analyzed data. ED and DM-C drafted the manuscript. All authors discussed the results and contributed to the final manuscript.

Data accessibility

The raw data supporting the conclusions of this manuscript will be made available by the authors, without undue reservation, to any qualified researcher.

Declaration of Competing Interests

The authors have no competing interests related to this work

Acknowledgement

This work was supported by the German Research Foundation (DFG, projects 389030878 and 405358801, to DMH, project 467228103 to ED, and project 407698736 to AF). DM-C was supported by a training grant of the International Graduate School of Neuroscience (IGSN), Ruhr-University Bochum during part of this work. We thank Sandra Lata and Britta Kaltwasser for technical support. For the maintenance of equipment, the authors are thankful to the IMCES (imaging center Essen) staff.

Supplementary materials

Supplementary material associated with this article can be found in the online version at doi:10.1016/j.matbio.2022.04.003.

Received 29 October 2021;
Received in revised form 21 March 2022;
Accepted 12 April 2022
Available online 14 April 2022

Keywords:
Astrocyte morphology;
Extracellular matrix;
Focal cerebral ischemia;
Glial scar;
Microglia;
Tenascin C

Abbreviations:
CSPG, chondroitin sulfate proteoglycan; DPI, days post ischemia; ECM, extracellular matrix; GFAP, glial fibrillary acidic protein; Iba1, ionized calcium-binding adapter molecule 1; ICAM1, intercellular adhesion molecule 1; MCAO, middle cerebral artery occlusion; TLR4, toll-like receptor 4; TNC, tenascin-C

[#]Equal contribution

References

[1] K.L. Adams, V. Gallo, The diversity and disparity of the glial scar, Nat. Neurosci. 21 (1) (2018) 9–15.
[2] S.A. Liddelow, B.A. Barres, Reactive astrocytes—Production, function, and therapeutic potential, Immunity 46 (6) (2017) 957–967.
[3] Joshua E. Burda, Michael V. Sofroniew, Reactive gliosis and the multicellular response to CNS damage and disease, Neuron 81 (2) (2014) 229–248.
[4] M.V. Sofroniew, Astrogliosis, Cold Spring Harbor perspectives in biology 7(2) (2015).
[5] M.E. Bianchi, DAMPs, PAMPs and alarmins—All we need to know about danger, J. Leukoc. Biol. 81 (1) (2007) 1–5.
[6] S.A. Liddelow, K.A. Guttenplan, L.E. Clarke, F.C. Bennett, C.J. Bohlen, L. Schirmer, M.L. Bennett, A.E. Münch, W.-S. Chung, T.C. Peterson, D.K. Wilton, A. Frouin, B.A. Napier, N. Panicker, M. Kumar, M.S. Buckwalter, D.H. Rowitch, V.L. Dawson, T.M. Dawson, B. Stevens, B.A. Barres, Neurotoxic reactive astrocytes are induced by activated microglia, Nature 541 (7638) (2017) 481–487.
[7] M.V. Sofroniew, H.V. Vinters, Astrocytes—Biology and pathology, Acta Neuropathol. 119 (1) (2010) 7–35.
[8] M.A. Anderson, J.E. Burda, Y. Ren, Y. Ao, T.M. O'Shea, R. Kawaguchi, G. Coppola, B.S. Khakh, T.J. Deming, M.V. Sofroniew, Astrocyte scar formation aids central nervous system axon regeneration, Nature 532 (7598) (2016) 195–200.
[9] G.E. Barreto, J. Gonzalez, Y. Torres, L. Morales, Astrocytic-neuronal crosstalk—Implications for neuroprotection from brain injury, Neurosci. Res. 71 (2) (2011) 107–113.
[10] L. Buscemi, M. Price, P. Bezzi, L. Hirt, Spatio-temporal overview of neuroinflammation in an experimental mouse stroke model, Sci. Rep. 9 (1) (2019) 507.
[11] L.L. Jones, R.U. Margolis, M.H. Tuszynski, The chondroitin sulfate proteoglycans neurocan, brevican, phosphacan, and versican are differentially regulated following spinal cord injury, Exp. Neurol. 182 (2) (2003) 399–411.
[12] S. Wiese, M. Karus, A. Faissner, Astrocytes as a source for extracellular matrix molecules and cytokines, Front. Pharmacol. 3 (120) (2012).
[13] R.A. Asher, P.S. Morgenstern Da Fau - Fidler, K.H. Fidler Ps Fau - Adcock, A. Adcock Kh Fau - Oohira, J.E. Oohira A Fau - Braistead, J.M. Braistead Je Fau - Levine, R.U. Levine Jm Fau - Margolis, J.H. Margolis Ru Fau - Rogers, J.W. Rogers Jh Fau - Fawcett, J.W. Fawcett, Neurocan is upregulated in injured brain and in cytokine-treated astrocytes, J. Neurosci. 20 (7) (2000) 2427–2438.
[14] S. Wiemann, J. Reinhard, A. Faissner, Immunomodulatory role of the extracellular matrix protein tenascin-C in neuroinflammation, Biochem. Soc. Trans. 47 (6) (2019) 1651–1660.
[15] V. Bellver-Landete, F. Bretheau, B. Mailhot, N. Vallières, M. Lessard, M.-E. Janelle, N. Vernoux, M.-È. Tremblay, T. Fuehrmann, M.S. Shoichet, S. Lacroix, Microglia are an essential component of the neuroprotective scar that forms after spinal cord injury, Nat. Commun. 10 (1) (2019) 518.
[16] J. Silver, The glial scar is more than just astrocytes, Exp. Neurol. 286 (2016) 147–149.
[17] Z. Liu, M. Chopp, Astrocytes, therapeutic targets for neuroprotection and neurorestoration in ischemic stroke, Prog. Neurobiol. 144 (2016) 103–120.
[18] Z. Liu, Y. Li, Y. Cui, C. Roberts, M. Lu, U. Wilhelmsson, M. Pekny, M. Chopp, Beneficial effects of gfap/vimentin reactive astrocytes for axonal remodeling and motor behavioral recovery in mice after stroke, Glia 62 (12) (2014) 2022–2033.
[19] M. Pekny, M. Pekna, Astrocyte reactivity and reactive astrogliosis—Costs and benefits, Physiol. Rev. 94 (4) (2014) 1077–1098.
[20] D. Qian, L. Li, Y. Rong, W. Liu, Q. Wang, Z. Zhou, C. Gu, Y. Huang, X. Zhao, J. Chen, Blocking Notch signal pathway suppresses the activation of neurotoxic A1 astrocytes after spinal cord injury, Cell Cycle 18 (21) (2019) 3010–3029.
[21] E. Dzyubenko, D. Manrique-Castano, C. Kleinschnitz, A. Faissner, D.M. Hermann, Role of immune responses for extracellular matrix remodeling in the ischemic brain, Ther. Adv. Neurol. Disord. 11 (2018) 1756286418818092.

[22] K. Takeuchi, N. Yoshioka, O. Higa, Chondroitin sulphate N-acetylgalactosaminyl-transferase-1 inhibits recovery from neural injury, Nat. Commun. 4 (2013).
[23] G.R. Choudhury, S. Ding, Reactive astrocytes and therapeutic potential in focal ischemic stroke, Neurobiol. Dis. 85 (2016) 234–244.
[24] E. Cekanaviciute, N. Fathali, K.P. Doyle, A.M. Williams, J. Han, M.S. Buckwalter, Astrocytic transforming growth factor-beta signaling reduces subacute neuroinflammation after stroke in mice, Glia 62 (8) (2014) 1227–1240.
[25] A. Faissner, L. Roll, U. Theocharidis, Tenascin-C in the matrisome of neural stem and progenitor cells, Mol. Cell. Neurosci. 81 (2017) 22–31.
[26] I. Kazanis, A. Belhadi, A. Faissner, C. ffrench-Constant, The adult mouse subependymal zone regenerates efficiently in the absence of tenascin-C, J. Neurosci. 27 (51) (2007) 13991–13996.
[27] E.D. Laywell, U. Dörries, U. Bartsch, A. Faissner, M. Schachner, D.A. Steindler, Enhanced expression of the developmentally regulated extracellular matrix molecule tenascin following adult brain injury, Proc. Natl. Acad. Sci. 89 (7) (1992) 2634–2638.
[28] K. Midwood, S. Sacre, A.M. Piccinini, J. Inglis, A. Trebaul, E. Chan, S. Drexler, N. Sofat, M. Kashiwagi, G. Orend, F. Brennan, B. Foxwell, Tenascin-C is an endogenous activator of Toll-like receptor 4 that is essential for maintaining inflammation in arthritic joint disease, Nat. Med. 15 (7) (2009) 774–780.
[29] H. Suzuki, M. Fujimoto, F. Kawakita, L. Liu, Y. Nakatsuka, F. Nakano, H. Nishikawa, T. Okada, H. Kanamaru, K. Imanaka-Yoshida, T. Yoshida, M. Shiba, Tenascin-C in brain injuries and edema after subarachnoid hemorrhage—Findings from basic and clinical studies, J. Neurosci. Res. 98 (1) (2020) 42–56.
[30] J. Reinhard, M. Renner, S. Wiemann, D.A. Shakoor, G. Stute, H.B. Dick, A. Faissner, S.C. Joachim, Ischemic injury leads to extracellular matrix alterations in retina and optic nerve, Sci. Rep. 7 (1) (2017) 43470.
[31] M. Fujimoto, M. Shiba, F. Kawakita, L. Liu, N. Shimojo, K. Imanaka-Yoshida, T. Yoshida, H. Suzuki, Effects of Tenascin-C knockout on cerebral vasospasm after experimental subarachnoid hemorrhage in mice, Mol. Neurobiol. 55 (3) (2018) 1951–1958.
[32] S. Wiemann, A. Yousf, S.C. Joachim, C. Peters, A.M. Mueller-Buehl, N. Wagner, J. Reinhard, Knock-out of tenascin-C ameliorates ischemia-induced rod-photoreceptor degeneration and retinal dysfunction, Front. Neurosci. 15 (2021) 642176.
[33] D. Manrique-Castano, E. Dzyubenko, M. Borbor, P. Vasileiadou, C. Kleinschnitz, L. Roll, A. Faissner, D.M. Hermann, Tenascin-C preserves microglia surveillance and restricts leukocyte and, more specifically, T cell infiltration of the ischemic brain, Brain Behav. Immun. 91 (2021) 639–648.
[34] M. Karus, B. Denecke, C. ffrench-Constant, S. Wiese, A. Faissner, The extracellular matrix molecule tenascin C modulates expression levels and territories of key patterning genes during spinal cord astrocyte specification, Development 138 (24) (2011) 5321–5331.
[35] E.M. York, J.M. LeDue, L.P. Bernier, B.A. MacVicar, 3DMorph automatic analysis of microglial morphology in three dimensions from ex vivo and in vivo imaging, eNeuro 5 (6) (2018).
[36] L.-P. Bernier, E.M. York, A. Kamyabi, H.B. Choi, N.L. Weilinger, B.A. MacVicar, Microglial metabolic flexibility supports immune surveillance of the brain parenchyma, Nat. Commun. 11 (1) (2020) 1559.
[37] M. D. M. Fernandez-Arjona, J.M. Grondona, P. Granados-Duran, P. Fernandez-Llebrez, M.D. Lopez-Avalos, Microglia morphological categorization in a rat model of neuroinflammation by hierarchical cluster and principal components analysis, Front. Cell. Neurosci. 11 (235) (2017).
[38] K.S. Midwood, M. Chiquet, R.P. Tucker, G. Orend, Tenascin-C at a glance, J. Cell Sci. 129 (23) (2016) 4321–4327.
[39] E. Favuzzi, A. Marques-Smith, R. Deogracias, C.M. Winterflood, A. Sánchez-Aguilera, L. Mantoan, P. Maeso, C. Fernandes, H. Ewers, B. Rico, Activity-dependent gating of parvalbumin interneuron function by the perineuronal net protein brevican, Neuron 95 (3) (2017) 639–655 e10.
[40] D. Rowlands, K.K. Lensjø, T. Dinh, S. Yang, M.R. Andrews, T. Hafting, M. Fyhn, J.W. Fawcett, G. Dick, Aggrecan directs extracellular matrix-mediated neuronal plasticity, J. Neurosci. 38 (47) (2018) 10102–10113.
[41] N. Thon, C.A. Haas, U. Rauch, T. Merten, R. Fässler, M. Frotscher, T. Deller, The chondroitin sulphate proteoglycan brevican is upregulated by astrocytes after entorhinal cortex lesions in adult rats, Eur. J. Neurosci. 12 (7) (2000) 2547–2558.
[42] A. Suttkus, S. Rohn, S. Weigel, P. Glöckner, T. Arendt, M. Morawski, Aggrecan, link protein and tenascin-R are essential components of the perineuronal net to protect neurons against iron-induced oxidative stress, Cell Death Dis. 5 (3) (2014) e1119.
[43] 2nd A.U. Joshi, P.S. Minhas, S.A. Liddelow, B. Haileselassie, K.I. Andreasson, G.W. Dorn, D. Mochly-Rosen, Fragmented mitochondria released from microglia trigger A1 astrocytic response and propagate inflammatory neurodegeneration, Nat. Neurosci. 22 (10) (2019) 1635–1648.
[44] X. Shi, L. Luo, J. Wang, H. Shen, Y. Li, M. Mamtilahun, C. Liu, R. Shi, J.-H. Lee, H. Tian, Z. Zhang, Y. Wang, W.-S. Chung, Y. Tang, G.-Y. Yang, Stroke subtype-dependent synapse elimination by reactive gliosis in mice, Nat. Commun. 12 (1) (2021) 6943.
[45] C. Gottschling, E. Dzyubenko, M. Geissler, A. Faissner, The indirect neuron-astrocyte coculture assay—An in vitro set-up for the detailed investigation of neuron-glia interactions, J. Vis. Exp. 117 (2016) e54757.
[46] Jean de Vellis, Cristina A. Ghiani, Ina B. Wanner, a.R. Cole, Protocols for neural cell culture, 2010.
[47] J. Yang, X. Zhang, X. Chen, L. Wang, G. Yang, Exosome mediated delivery of miR-124 promotes neurogenesis after ischemia, Mol. Ther. 7 (2017) 278–287.
[48] W.P. Yew, N.D. Djukic, J.S.P. Jayaseelan, F.R. Walker, K.A.A. Roos, T.K. Chataway, H. Muyderman, N.R. Sims, Early treatment with minocycline following stroke in rats improves functional recovery and differentially modifies responses of peri-infarct microglia and astrocytes, J. Neuroinflamm. 16 (1) (2019) 6.
[49] M. Iwai, G. Cao, W. Yin, R.A. Stetler, J. Liu, J. Chen, Erythropoietin promotes neuronal replacement through revascularization and neurogenesis after neonatal hypoxia/ischemia in rats, Stroke 38 (10) (2007) 2795–2803.
[50] E. Garcion, A. Halilagic, A. Faissner, C. ffrench-Constant, Generation of an environmental niche for neural stem cell development by the extracellular matrix molecule tenascin C, Development 131 (14) (2004) 3423–3432.

[51] A. Dobbertin, S. Czvitkovich, U. Theocharidis, J. Garwood, M.R. Andrews, F. Properzi, R. Lin, J.W. Fawcett, A. Faissner, Analysis of combinatorial variability reveals selective accumulation of the fibronectin type III domains B and D of tenascin-C in injured brain, Exp. Neurol. 225 (1) (2010) 60–73.
[52] L. Roll, U.T. Eysel, A. Faissner, Laser lesion in the mouse visual cortex induces a stem cell niche-like extracellular matrix, produced by immature astrocytes, Front. Cell. Neurosci. 14 (102) (2020) 102.
[53] D.A. Steindler, D. Settles, H.P. Erickson, E.D. Laywell, A. Yoshiki, A. Faissner, M. Kusakabe, Tenascin knockout mice—Barrels, boundary molecules, and glial scars, J. Neurosci. 15 (3) (1995) 1971–1983 Pt 1.
[54] J.E. Holley, D. Gveric, J.L. Whatmore, N.J. Gutowski, Tenascin C induces a quiescent phenotype in cultured adult human astrocytes, Glia 52 (1) (2005) 53–58.
[55] H.P. Erickson, J.L. Inglesias, A six-armed oligomer isolated from cell surface fibronectin preparations, Nature 311 (5983) (1984) 267–269.
[56] R.A. Kammerer, T. Schulthess, R. Landwehr, A. Lustig, D. Fischer, J. Engel, Tenascin-C hexabrachion assembly is a sequential two-step process initiated by coiled-coil α-Helices *, J. Biol. Chem. 273 (17) (1998) 10602–10608.
[57] L. De Laporte, J.J. Rice, F. Tortelli, J.A. Hubbell, Tenascin C promiscuously binds growth factors via its fifth fibronectin Type III-like domain, PLoS One 8 (4) (2013) e62076.
[58] R.P. Tucker, R. Chiquet-Ehrismann, Tenascin-C—Its functions as an integrin ligand, Int. J. Biochem. Cell Biol. 65 (2015) 165–168.
[59] J.M. Day, A.I. Olin, A.D. Murdoch, A. Canfield, T. Sasaki, R. Timpl, T.E. Hardingham, A. Aspberg, Alternative splicing in the aggrecan G3 domain influences binding interactions with tenascin-C and other extracellular matrix proteins, J. Biol. Chem. 279 (13) (2004) 12511–12518.
[60] A. Giuffrida, S. Scarpa, P. Birarelli, A. Modesti, The interaction of tenascin-C with fibronectin modulates the migration and specific metalloprotease activity in human mesothelioma cell lines of different histotype, Int. J. Oncol. 25 (3) (2004) 745–750.
[61] S. Soleman, P.K. Yip, D.A. Duricki, L.D.F. Moon, Delayed treatment with chondroitinase ABC promotes sensorimotor recovery and plasticity after stroke in aged rats, Brain 135 (Pt 4) (2012) 1210–1223.
[62] E. Dzyubenko, C. Gottschling, A. Faissner, Neuron-Glia interactions in neural plasticity—Contributions of neural extracellular matrix and perineuronal nets, Neural Plast. 2016 (2016) 5214961.
[63] R.G. Mestriner, L. Saur, P.B. Bagatini, P.P.A. Baptista, S.P. Vaz, K. Ferreira, S.A. Machado, L.L. Xavier, C.A. Netto, Astrocyte morphology after ischemic and hemorrhagic experimental stroke has no influence on the different recovery patterns, Behav. Brain Res. 278 (2015) 257–261.
[64] C. Escartin, E. Galea, A. Lakatos, J.P. O'Callaghan, G.C. Petzold, A. Serrano-Pozo, C. Steinhäuser, A. Volterra, G. Carmignoto, A. Agarwal, N.J. Allen, A. Araque, L. Barbeito, A. Barzilai, D.E. Bergles, G. Bonvento, A.M. Butt, W.-T. Chen, M. Cohen-Salmon, C. Cunningham, B. Deneen, B. De Strooper, B. Díaz-Castro, C. Farina, M. Freeman, V. Gallo, J.E. Goldman, S.A. Goldman, M. Götz, A. Gutiérrez, P.G. Haydon, D.H. Heiland, E.M. Hol, M.G. Holt, M. Iino, K.V. Kastanenka, H. Kettenmann, B.S. Khakh, S. Koizumi, C.J. Lee, S.A. Liddelow, B.A. MacVicar, P. Magistretti, A. Messing, A. Mishra, A.V. Molofsky, K.K. Murai, C.M. Norris, S. Okada, S.H.R. Oliet, J.F. Oliveira, A. Panatier, V. Parpura, M. Pekna, M. Pekny, L. Pellerin, G. Perea, B.G. Pérez-Nievas, F.W. Pfrieger, K.E. Poskanzer, F.J. Quintana, R.M. Ransohoff, M. Riquelme-Perez, S. Robel, C.R. Rose, J.D. Rothstein, N. Rouach, D.H. Rowitch, A. Semyanov, S. Sirko, H. Sontheimer, R.A. Swanson, J. Vitorica, I.-B. Wanner, L.B. Wood, J. Wu, B. Zheng, E.R. Zimmer, R. Zorec, M.V. Sofroniew, A. Verkhratsky, Reactive astrocyte nomenclature, definitions, and future directions, Nat. Neurosci. 24 (3) (2021) 312–325.
[65] V. Haage, N. Elmadany, L. Roll, A. Faissner, D.H. Gutmann, M. Semtner, H. Kettenmann, Tenascin C regulates multiple microglial functions involving TLR4 signaling and HDAC1, Brain Behav. Immun. 81 (2019) 470–483.
[66] A.M. Marzeda, K.S. Midwood, Internal affairs—Tenascin-C as a clinically relevant, endogenous driver of innate immunity, J. Histochem. Cytochem. 66 (4) (2018) 289–304.
[67] L.R. Liu, J.C. Liu, J.S. Bao, Q.Q. Bai, G.Q. Wang, Interaction of microglia and astrocytes in the neurovascular unit, Front. Immunol. 11 (2020).
[68] I. Enlimomab, Acute stroke trial, use of anti-ICAM-1 therapy in ischemic stroke, Neurology 57 (8) (2001) 1428.
[69] O. Steiner, C. Coisne, R. Cecchelli, R. Boscacci, U. Deutsch, B. Engelhardt, R. Lyck, Differential roles for endothelial ICAM-1, ICAM-2, and VCAM-1 in shear-resistant T cell arrest, polarization, and directed crawling on blood—brain barrier endothelium, J. Immunol. 185 (8) (2010) 4846–4855.
[70] H. Wee, H.-M. Oh, J.-H. Jo, C.-D. Jun, ICAM-1/LFA-1 interaction contributes to the induction of endothelial cell-cell separation—Implication for enhanced leukocyte diapedesis, Exp. Mol. Med. 41 (5) (2009) 341–348.
[71] A.M.M. Thinn, Z. Wang, D. Zhou, Y. Zhao, B.R. Curtis, J. Zhu, Autonomous conformational regulation of $\beta_3$integrin and the conformation-dependent property of HPA-1a alloantibodies, Proc. Natl. Acad. Sci. 115 (39) (2018) E9105–E9114.
[72] R. Lagos-Cabré, A. Alvarez, M. Kong, F. Burgos-Bravo, A. Cárdenas, E. Rojas-Mancilla, R. Pérez-Nuñez, R. Herrera-Molina, F. Rojas, P. Schneider, M. Herrera-Marschitz, A.F.G. Quest, B. van Zundert, L. Leyton, αVβ3 Integrin regulates astrocyte reactivity, J. Neuroinflamm. 14 (1) (2017) 194.
[73] E. Forsberg, E. Hirsch, L. Fröhlich, M. Meyer, P. Ekblom, A. Aszodi, S. Werner, R. Fässler, Skin wounds and severed nerves heal normally in mice lacking tenascin-C, Proc. Natl. Acad. Sci. 93 (13) (1996) 6594–6599.
[74] W. Clark, N. Lessov, M. Dixon, F. Eckenstein, Monofilament intraluminal middle cerebral artery occlusion in the mouse, Neurol. Res. 19 (6) (1997) 641–648.
[75] A. Faissner, J. Kruse, J1/tenascin is a repulsive substrate for central nervous system neurons, Neuron 5 (5) (1990) 627–637.